Elastic Scattering of 20.35-Mev Protons by Zn^{64}, Zn^{66}, and Zn^{68}[†]

R. W. Boom* AND J. Reginald Richardson
Department of Physics, University of California, Los Angeles, California
(Received April 27, 1959)

The absolute differential cross section for the elastic scattering of (20.35±0.25)-Mev protons has been measured for enriched Zn^{64}, Zn^{66}, and Zn^{68} foils. In the angular range of 30°–160° about 50 measurements were made for each foil (spaced from 1° to 5°) to an estimated accuracy of about 5% standard deviation. Scattered protons were detected by nuclear emulsions wrapped around a 4-in. diameter scattering chamber, all angles being exposed simultaneously. Detector energy resolution is 2.5%, angular resolution is 1° standard deviation, and relative angular shifts are determined to 0.1°. Correction has been made for the finite sizes of beam and detector and for multiple scattering in the target and in the detector stopper. The ±0.25-Mev energy spread includes maximum and minimum energies due to beam drift, beam spread, and target foil thickness. Three minima are found for each isotope: Zn^{64} at 63°, 104°, 142°; Zn^{66} at 62°, 102.5°, 142°; and Zn^{68} at 61°, 101°, 142°. The absolute cross sections are approximately the same except at the third minima, where for Zn^{64}, Zn^{66}, and Zn^{68} they are respectively, 1.46, 1.07, and 0.61 mb/sterad.

INTRODUCTION

DIFFERENTIAL elastic scattering of protons has been measured by investigators in the 10–40 Mev energy region[1] and analyzed using the optical model potential.[2] Most experiments have been done with isotope mixtures according to natural abundances so that nuclei of various radii are present in the target. It is thus of interest to see if scattering from different isotopes will yield additional information concerning nuclear parameters. Zinc is an appropriate choice because the spread in mass number is large for such a light element. In addition, theoretical fits have been quite successful for zinc. Preliminary reports on this work have been given previously.[3]

EXPERIMENT

The external beam from the UCLA synchrocyclotron was directed into the 4-in. diameter scattering chamber,

† Assisted jointly by the Office of Naval Research and the U. S. Atomic Energy Commission. Part of a dissertation submitted by R. W. Boom for the Ph.D. degree at the University of California at Los Angeles.
* Now guest physicist at the Institute for Nuclear Physics of the Friedrich-Wilhelms University, Bonn, Germany.
[1] Several in the 10–40 Mev range: J. W. Burkig and B. T. Wright, Phys. Rev. 82, 451 (1951); B. T. Wright, University of California Radiation Laboratory Report UCRL-2422, November, 1953 (unpublished); B. L. Cohen and R. V. Neidigh, Phys. Rev. 93, 282 (1954); B. B. Kinsey and T. Stone, Phys. Rev. 103, 975 (1956); J. Leahy, University of California Radiation Laboratory Report UCRL-3273, February, 1956 (unpublished); I. E. Dayton and G. Schrank, Phys. Rev. 101, 1358 (1956); M. M. Hintz, Phys. Rev. 106, 1201 (1957); N. S. Wall and W. F. Waldorf, Phys. Rev. 107, 1602 (1957); Gibson, Prowse, and Rotblat, Proc. Roy. Soc. (London) 243, 237 (1957); R. H. Chow and B. T. Wright, Can. J. Phys. 35, 184 (1957); M. M. Hintz, Bull. Am. Phys. Soc. Ser. II, 2, 14 (1957); M. K. Brussel and J. H. Williams, *Proceedings of the University of Pittsburgh Conference on Nuclear Structure, 1957*, edited by S. Meshkov (University of Pittsburgh and Office of Ordnance Research, U. S. Army, 1957), p. 34; John H. Williams and M. K. Brussel, Phys. Rev. 110, 136 (1958).
[2] Saxon, Melkanoff, Nodvik, and Woods, Phys. Rev. 95, 577 (1954); 100, 1805 (1955); 106, 793 (1957). Glassgold, Cheston, Stein, Schuldt, and Erickson, Phys. Rev. 106, 1207 (1957); 107, 1372 (1957); 109, 1201 (1958).
[3] R. W. Boom and H. A. Howe, Bull. Am. Phys. Soc. Ser. II, 2, 305 (1957); R. W. Boom and J. R. Richardson, Bull. Am. Phys. Soc. 3, 419 (1958).

at the center of which was positioned a foil holder at 45° to the incoming beam for simultaneous recording at all angles. The scattered protons left the chamber through thin windows at the median plane, passed through thin aluminum absorbers staggered around the circumference, were further slowed down by the thick front surface of the film holders, and stopped in the nuclear emulsion. Since the nuclear emulsion was laid along a circumference, protons were perpendicularly incident; thus elastic scattering cross sections are proportional to film-surface elastic-scattering track densities. Scattering angles are proportional to linear distances along the film and are determined from several 1° wide blank spaces on each exposed trace; these "no proton" blank spaces are behind thick vertical brass strips soldered on the external absorber holder.

The divergence of the beam (as defined by the $\frac{3}{8}$-in. $\times\frac{1}{16}$-in. slit) in angle and energy is measured behind a vacuum extension pipe with a Faraday cup and movable slit. The angular divergence of the beam (as defined by a $\frac{3}{8}$-in.$\times\frac{1}{16}$-in. slit) for an approximate Gaussian current distribution was 0.2° rms deviation and the variation of the mean energy in the horizontal direction was ±100 kev high in the center and dropping on both sides. No vertical energy variation was found.

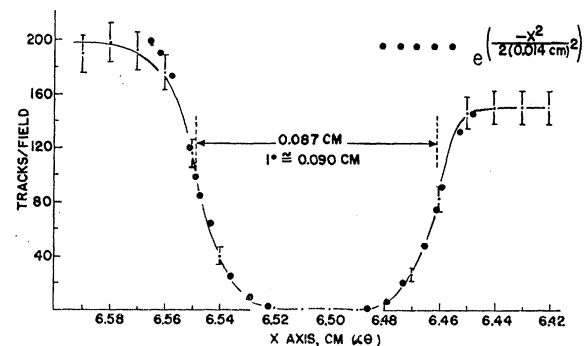Careful alignment and centering of the scattering

FIG. 1. Counting rate behind an index wire. The expected Gaussian distribution is shown by the circles.

TABLE I. The isotopic composition of the foils.

				Atomic %							
	Zn^{64}	Zn^{66}	Zn^{67}	Zn^{68}	Zn^7	Na	Mg	Cu	Cd	Ag	Si
1	93.12±0.06	6.29±0.05	0.159±0.003	0.432±0.009	<0.10	<0.04					
2	10.0 ±0.7	78.4 ±3.0	1.2 ±0.2	8.8 ±1.0	1.6 ±1.0		<0.02	<0.04	<0.15		
3	2.7 ±0.2	2.8 ±0.2	0.4 ±0.1	93.9 ±0.5	0.3 ±0.1		<0.04			<0.04	<0.02

chamber with respect to the beam and accurate measurement of the angles of the various index strips allowed absolute angles to be measured with an accuracy of ±0.2°; angles relative to the index strip shadows are better than ±0.1°.
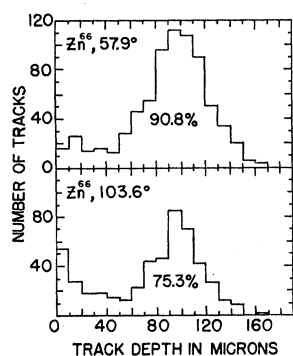
The nuclear emulsion, Ilford E1, is 300 μ thick mounted on 0.008-in. celluloid backing. The film holders are rigid cylindrical sections, spaced to clear the side slits and locked in place on a vertical bar. The front surface is 0.050-inch Al, most of the absorber required to stop the scattered protons in the film. Behind this front surface is a 0.004-inch sheet of black polyvinylchloride which serves as a light seal and is inert to the

FIG. 2. Representative number-range histograms showing the separation of elastic and inelastic scattering peaks.

emulsion surface. Two films were used (for front and back quadrants) with considerable overlap near 90°.

The three zinc foils, supplied by the Isotope Division, Oak Ridge National Laboratory, are approximately 10 mg/cm² thick, and as measured by scanning with soft Cu x-rays are known to ±1.6%. As foils, these samples are of poor quality; the above error is a conservative estimate based on pinhole density and size in relation to beam size. The composition of the foils is shown in Table I.

PROCEDURE

Three exposures (one for each foil) were made on each film. Before and after the exposures beam energy, alignment, and current integration are checked. The Faraday cup feed-back electrometer circuit was that described by Caldwell and Royden,[4] and was calibrated by their current-time method. The effective proton energy for the elastic scattering, including beam drift, spread, and zinc foil thickness was 20.35±0.25 Mev, as found from the ranges in aluminum reported by Bichsel,

[4] D. O. Caldwell and H. N. Royden, Rev. Sci. Instr. 27, 91 (1956).

Mozley, and Aron.[5] The developed emulsions were mounted on a special stage with 11×11 cm² movement and tracks were counted and analyzed under 900× magnification. First the index strips are located on each trace by counting behind the strips; Fig. 1 is a typical example. Next three depth-number histograms, evenly spaced, are taken between each set of index strips. Finally, top surface track density is counted between the histogram points. To be counted, a track must enter the film at a sufficiently small angle and must end properly. Two of the histograms are shown in Fig. 2, each with a different inelastic scattering fraction. Interpolated inelastic scattering corrections can be made from these graphs for the intervening top surface points. The inelastic scattering fraction can, in most cases, be determined to better than 1% due to the $2\frac{1}{2}\%$ energy resolution of the detector and the fact that the three enriched foils are for zinc isotopes whose first excited levels are at about 1 Mev. Figure 3 is an exposure made to check the range-energy calibration of the emulsion and clearly shows the ease in separating elastic from inelastic scattering.

The detector area is defined by a sequence of adjacent squares, each being determined by a 10×10 whipple disk mounted in one of the microscope oculars. These areas are measured to ±1.2%.

In addition to the inelastic correction or interpolated inelastic correction described above, three other corrections are applied to the data. These account for multiple scattering in the aluminum abosrber in front of the film, multiple scattering in the zinc target foils, and for finite geometry. The final relation between the number of elastic protons counted Y_0 and the scattering cross
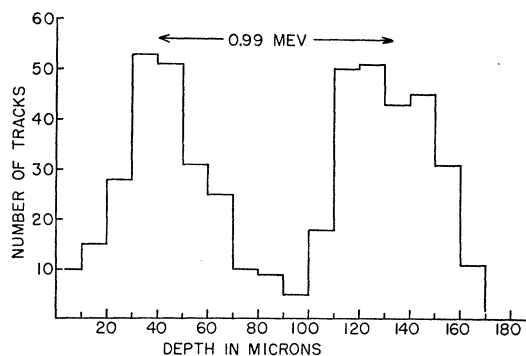

FIG. 3. Energy calibration of the film. Proton peaks for elastic scattering and for inelastic scattering from the 0.99-Mev level of Zn^{64}.

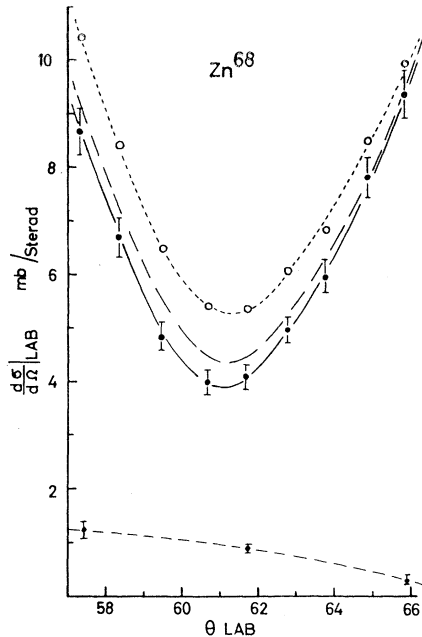[5] Bichsel, Mozley, and Aron, Phys. Rev. 105, 1788 (1957).

FIG. 4. Corrections at the first minimum for Zn^{68}. The top dotted curve is from the surface track counting. The next dashed curve shows the results of the subtraction of the inelastic scattering contribution. The solid curve shows the final results after the other corrections are made. The bottom dashed curve shows the inelastic scattering contribution.

section is

$$Y_0 = \frac{tN_0}{\bar{A}}\sigma(\theta_0)Q\frac{2w_0 2h}{R^2}\left(\frac{1+\Delta_2}{1+\Delta_1}\right)(1+\Delta_3+\Delta_4+\Delta_5).$$

Here $\sigma(\theta_0)$ is the differential elastic scattering cross section in $cm^2/sterad$, θ_0 is the scattering angle defined from the center of the foil to the center of the detector, t the zinc thickness in g/cm^2, N_0 Avogadro's number, $\bar{A}$ the average atomic weight for the target, Q the total number of protons, $2w_0$ detector width, $2h$ detector height, R film radius, and the Δ's are the various corrections. The solid angle term $2w_0 2h/R^2$ is not used directly, but instead is found from the angular calibration of the

TABLE II. Summary of experimental errors.

Source	Term	Standard deviation[a]
Number of tracks counted (includes inelastic subtraction)	dY_0/Y_0	~0.04
Correction procedure	$d\Delta/\Delta$	≤0.01
Uncertainty in average atomic number	dA/A	~0.002
Foil thickness	dt/t	0.016
Ratio detector height/width	df/f	≤0.008
Detector width in radians	$2d\theta_x/\theta_x$	0.016
Total beam current	dQ/Q	0.005
Combined standard deviation		~0.05

[a] Most of the points have a statistical deviation of 5%, a few as low as 3%, and a few around 8% at the second and third minima where the inelastic scattering correction was high. Separate standard deviations are given for each point in Table III.

film in the various regions between index wires. This method eliminates the necessity to measure R and automatically accounts for noncircular deviations in the chamber and film holder.

Δ_1, the correction for multiple scattering in the aluminum absorber in front of the film, is $-\frac{1}{2}\langle X^2\rangle n^{-1}d^2n/dX^2$, where n is the track density, X is the linear distance along film, and $\langle X^2\rangle$ is the rms deviation at the film surface. By using the Rossi-Greisen[6] formula for correlating multiple-scattering angle with lateral displacement in conjunction with the film energy calibration of Fig. 3, the lateral displacement of protons on the
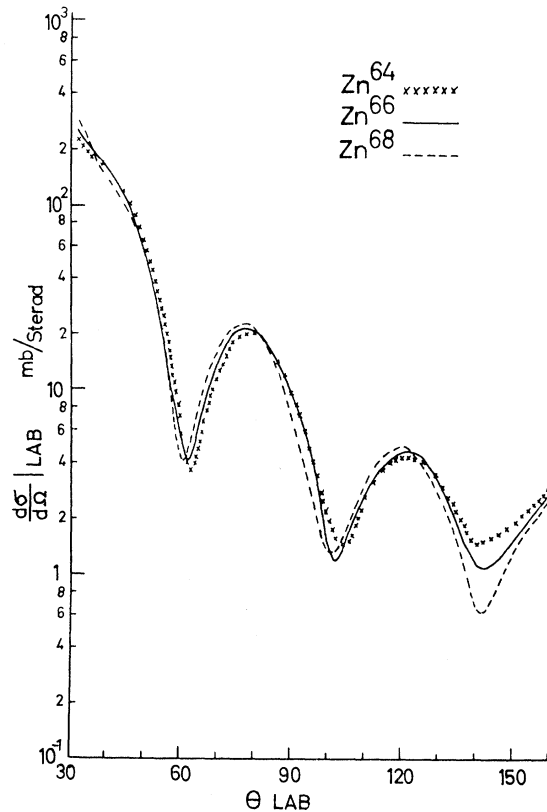

FIG. 5. The final elastic scattering cross sections for protons of 20.35-Mev energy.

film surface is calculated to be approximately Gaussian with $(\langle X^2\rangle)^{\frac{1}{2}}=0.014$ cm. This value is roughly confirmed by counting behind the edge of an index strip stopper as shown in Fig. 1. The slit height in front of the films is $\frac{1}{8}$ in.; because of the small value of $\langle X^2\rangle$ these slit edges in no way affect the counting rates at the center of the exposed trace. By putting most of the aluminum absorber in contact with the film, Δ_1 is decreased and, in this case, never exceeded ±0.0015.

Multiple scattering in the zinc target foils is corrected by an expression due to Chase and Cox[7] and here used

[6] B. Rossi and K. Greisen, Revs. Modern Phys. 13, 249 (1941).
[7] C. T. Chase and R. T. Cox, Phys. Rev. 58, 246 (1940).

TABLE III. Elastic cross sections for 20.35-Mev protons.

Foil enriched in Zn[64]

θ Lab	dσ/dΩ mb/sterad	Standard deviation	θ Lab	dσ/dΩ mb/sterad	Standard deviation
32.0	222	13	101.3	1.89	0.12
35.2	183	10	102.6	1.50	0.09
38.5	171	9	103.9	1.44	0.08
41.5	134	6	104.8	1.46	0.09
44.7	120	7	105.7	1.48	0.09
50.9	57.0	2.8	107.1	1.63	0.11
56.3	20.6	0.9	108.5	2.21	0.11
56.5	19.2	1.0	112.5	3.09	0.16
58.0	13.0	0.7	114.8	3.71	0.19
59.5	8.06	0.44	116.3	4.09	0.21
60.6	5.95	0.32	119.4	4.38	0.23
61.6	4.26	0.23	120.4	4.43	0.22
62.9	3.60	0.18	122.1	4.19	0.21
63.7	4.12	0.19	123.9	4.41	0.23
65.3	5.23	0.24	125.4	4.09	0.21
66.5	6.78	0.35	128.4	3.87	0.21
70.3	11.8	0.6	129.9	3.57	0.20
74.0	18.0	0.8	134.1	2.52	0.14
76.7	18.7	0.8	137.3	1.94	0.15
78.9	20.7	0.9	138.9	1.56	0.13
81.2	19.7	1.0	140.8	1.46	0.13
82.3	18.9	0.8	142.0	1.59	0.12
83.4	16.8	0.9	144.0	1.63	0.14
85.7	15.7	0.6	146.4	1.75	0.15
88.2	12.1	0.7	148.0	1.62	0.11
92.4	6.91	0.46	150.9	2.05	0.16
95.7	4.65	0.21	155.5	2.38	0.18
96.9	3.60	0.21	158.1	2.24	0.12
98.9	2.40	0.16	160.0	3.03	0.21

Foil enriched in Zn[66]

θ Lab	dσ/dΩ mb/sterad	Standard deviation	θ Lab	dσ/dΩ mb/sterad	Standard deviation
32.0	255	13	103.6	1.24	0.09
35.1	191	11	104.7	1.43	0.09
38.9	172	8	105.8	1.70	0.10
41.5	139	7	108.4	1.98	0.11
44.9	110	6	112.5	3.68	0.18
50.9	49.2	2.7	114.8	3.68	0.21
56.5	13.7	0.8	118.7	4.21	0.22
57.9	11.8	0.5	120.0	4.56	0.24
60.1	5.80	0.31	122.5	4.55	0.23
62.2	4.02	0.20	123.8	4.74	0.27
64.3	4.94	0.25	125.3	4.07	0.21
66.4	8.13	0.38	128.2	3.39	0.21
70.2	14.4	0.8	129.8	3.32	0.16
74.0	19.4	1.1	133.7	2.46	0.14

Foil enriched in Zn[66] (continued)

θ Lab	dσ/dΩ mb/sterad	Standard deviation	θ Lab	dσ/dΩ mb/sterad	Standard deviation
78.4	20.6	1.1	137.1	1.47	0.12
81.4	21.6	1.1	138.6	1.42	0.11
83.5	15.9	0.8	141.6	1.07	0.06
88.2	11.9	0.7	142.6	1.15	0.09
88.6	10.7	0.6	146.0	1.22	0.09
93.6	6.67	0.37	147.6	1.25	0.11
95.7	4.20	0.21	150.4	1.59	0.11
96.9	2.93	0.19	154.9	2.13	0.15
99.0	1.82	0.13	157.2	2.24	0.12
101.3	1.29	0.11	159.5	2.56	0.18
102.4	1.17	0.08			

Foil enriched in Zn[68]

θ Lab	dσ/dΩ mb/sterad	Standard deviation	θ Lab	dσ/dΩ mb/sterad	Standard deviation
32.1	279	15	91.8	5.03	0.32
35.3	192	11	95.7	2.76	0.16
38.5	148	8	96.3	2.47	0.14
41.6	123	6	98.9	1.53	0.10
44.7	103	5	100.8	1.41	0.10
51.0	48.8	2.7	102.4	1.31	00.9
56.3	12.5	0.5	104.1	1.41	0.09
56.4	10.7	0.5	105.2	1.81	0.11
57.4	8.63	0.43	108.5	2.47	0.12
58.4	6.70	0.37	111.9	3.67	0.17
59.5	4.85	0.26	114.1	3.96	0.26
60.7	3.97	0.23	116.4	4.24	0.25
61.7	4.20	0.23	118.6	4.47	0.22
62.8	4.96	0.24	120.3	5.19	0.27
63.8	5.95	0.30	121.4	4.78	0.23
64.9	7.78	0.36	123.2	4.21	0.23
65.9	9.33	0.46	125.4	3.78	0.20
66.8	11.0	0.5	127.7	3.29	0.18
69.2	14.2	0.7	129.9	2.67	0.13
70.3	16.5	0.9	131.0	2.56	0.15
71.4	17.9	0.8	133.9	1.87	0.09
73.5	20.4	0.9	136.6	1.24	0.09
75.7	21.4	0.9	140.0	0.66	0.06
77.9	23.8	1.1	141.1	0.68	0.06
80.1	20.4	1.0	142.8	0.61	0.04
82.6	17.5	0.7	144.5	0.73	0.06
84.5	14.8	0.6	145.6	0.81	0.07
87.9	10.5	0.5	150.1	1.36	0.09
88.8	8.49	0.42	154.6	1.82	0.13
			159.0	2.35	0.13

in the form

$$\Delta_2 = \tfrac{1}{4}\left(\cot\theta_0\frac{\sigma'(\theta_0)}{\sigma(\theta_0)} + \frac{\sigma''(\theta_0)}{\sigma(\theta_0)}\right)\left[\frac{1}{\sin\varphi} - \frac{1}{\sin(\theta_0\pm\varphi)}\right]\langle\theta^2\rangle,$$

where the $+$ in the denominator is used for reflection angles (85°–160° film), and the $-$ for transmission angles (30°–95° film); σ' is $d\sigma(\theta_0)/d\theta$, σ'' is $d^2\sigma(\theta_0)/d\theta^2$, φ is the angle between the plane of the zinc foil and the beam, and $\langle\theta^2\rangle$ is the rms deviation for multiple scattering for half of the foil thickness. Δ_2 is less than ±0.004, except near the first, second, and third minima where it becomes +0.04, +0.01, and +0.01, respectively.

The final and largest corrections account for the finite size of beam, the Gaussian nature of the beam current, the angular divergence of the beam, and the finite detector size. As adapted from Dayton and Schrank,[8] they are

$$\Delta_3 = \frac{1}{2R_0^2}[(9c^2-3)d^2 - w^2 - h^2 - b^2],$$

$$\Delta_4 = \frac{1}{2R_0^2}\frac{\sigma'(\theta_0)}{\sigma(\theta_0)}\left[\cot\theta_0 + \left(\frac{h^2+b^2}{3}\right) + 6CSd^2\right],$$

$$\Delta_5 = \frac{1}{2R_0^2}\frac{\sigma''(\theta_0)}{\sigma(\theta_0)}[w^2 + S^2d^2],$$

where σ, σ', σ'', φ, and θ_0 are defined above, R_0 is the chamber radius, d^2 is the rms deviation of the beam on the zinc foil, $2w$ is the projected detector width at the chamber circumference, $2h$ is the detector height, $2b$ is the beam height at the zinc foil, C_0 is $\cos\theta_0$, S_0 is $\sin\theta_0$, C is $\cos(\theta_0-\varphi)$, and S is $\sin(\theta_0-\varphi)$. Δ_3 is small

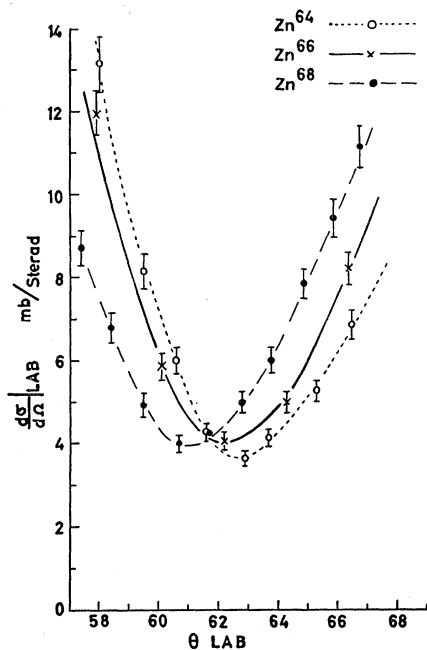[8] I. E. Dayton and G. Schrank, Phys. Rev. 101, 1358 (1956).

FIG. 6. Details of the measurements near the first minimum in the elastic scattering cross section.

and varies from -0.0058 to -0.0070 with b^2 the dominant term. Δ_4, the first derivative term, varies from -0.03 at $30°$ and $160°$ to $+0.01$ at the minima and depends mostly on $2b$, the beam height. Δ_5, the largest correction, is the second derivative term and reaches a maximum of $+0.08$ at the first minima. The only large dimension, b, does not appear in the expression for Δ_5 so that a large slit height can be used to get the most beam without sacrificing accuracy.

The product of all corrections is 0.90 at the first minima, 1.02 at $30°$ and $160°$, and follows the shape of $\sigma(\theta_0)$ between. While these corrections are high, it should be noted that the corrections do not affect the angular positions of the diffraction patterns. The corrections raise maxima and decrease minima as indicated in Fig. 4, where a summary of the largest corrections found, Zn^{68} at the first minimum, are graphed. Table II shows a summary of the sources of the experimental error.

Values for cross sections and derivatives in the above corrections are averages over an angular interval of $1°$ rms deviation (the current intensity is approximately Gaussian on the zinc foils). Except at the first minima, these functions vary so slowly with angle that the resulting cross sections are independent of this angular resolution. This is not true at the first minima and the true cross sections here may be 1 or 2% lower than those found.

RESULTS

Cross sections are given in Table III and Fig. 5. Cross sections for the three foils are seen to be most

different at the third minimum; for Zn^{64}; Zn^{66}, and Zn^{68} they are, respectively, 1.46, 1.07, and 0.61 mb/sterad, where surprisingly all minima appear at the same angle, $142°$. Even though the third minima are quite broad, sufficient points were taken to detect the expected shifts. Figures 6 and 7 show that at the first minimum the angular shift per isotope is about $1°$ and at the second minimum the shift is about $1.5°$ per isotope; in both cases, the Zn^{68} minimum is at the smallest angle and Zn^{64} at the largest angle. The angular positions of the first two minima, as well as the angular shift per isotope, are quite well predicted by the $1/KR$ empirical relations found by Dayton and Schrank.[8]

Preliminary analysis by the UCLA theoretical group[9] indicates that the results can be fitted with the addition
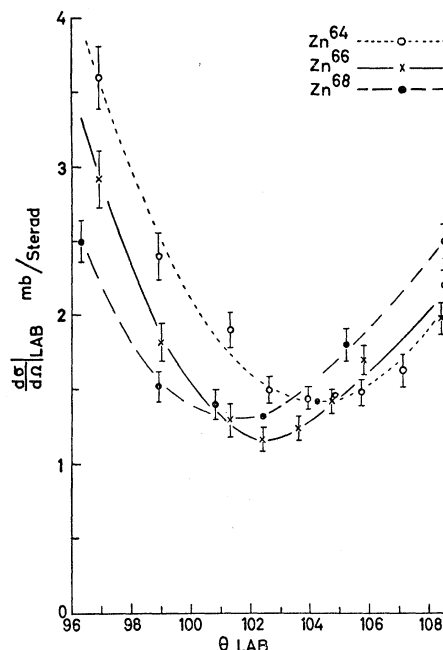

FIG. 7. Details of the measurements near the second minimum in the elastic scattering cross section.

of a spin-orbit term. It is expected, however, that different parameters (in addition to the different atomic weights A) will have to be used for the different isotopes, particularly to fit the third minima.

[9] Saxon, Melkanoff, and Nodvick (private communication).